A statistically-based method to estimate long-term daily air temperature at high elevations

Marco Bongio[1,2], Giovanni Baccolo[3], Riccardo Scotti[2], Carlo De Michele[1]

[1]Department of Civil and Environmental Engineering, Politecnico di Milano, Piazza Leonardo da Vinci 32, 20133, Milano, Italy

[2]Servizio Glaciologico Lombardo, Via Statale 43, 23888 La Valletta Brianza (LC), Italy, riccardoscotti80@gmail.com

[3]Dipartimento di Scienze, Università di Roma Tre, via Marconi 446,00146 Roma, Italy, giovanni.baccolo@uniroma3.it

Correspondence to: Bongio Marco (marco.bongio@polimi.it) and Carlo De Michele (carlo.demichele@polimi.it)

Keywords: Consistency, stationarity, trend removal, Ensemble, KGE, European Alps, high elevation sites, statistical model, long-term daily temperature time series, Temperature Lapse Rate, Residuals' statistical distributions.

Abstract. Air temperature is a pivotal variable influencing numerous chemical, physical, hydrological and biological processes, however there is a scarcity of long-term data, especially at high elevations. This study proposes a statistical methodology to reconstruct daily air temperature time series at a high elevation site, Jungfraujoch (3571 m a.s.l.) involving observations from 30 MeteoSwiss stations located at lower-altitude (485-2691 m a.s.l.), with uninterrupted observations within the period 1971-2023. The reconstructed time series has been compared with those extracted from two gridded datasets: HISTALP and the one provided by Imfeld et al. (2023). We found that: i) The selection of stations with temporally consistent long-term observations is a critical issue; ii) Model performance, efficiency, and errors are primarily influenced by elevation; iii) The Kling-Gupta Efficiency (KGE) resulted an appropriate metric to define the ensemble simulation; iv) Comparable performance with existing datasets, but with greater computational efficiency; v) The estimated time series may represent a benchmark for evaluating observational anomalies and for deeper analysis of Elevation-Dependent Warming issue.

1. INTRODUCTION

Atmospheric temperature is the measurement of the average kinetic energy of the molecules constituting the air, it plays a key role in radiative, dynamical, and chemical processes in the atmosphere and is the main variable of atmospheric sciences. Surface air temperature is conventionally measured at the height of 2 m above ground (WMO 2023) and is the main driver of many Earth system processes: 1) life cycles and traits' evolution (Sheldon and Tewksbury, 2014); 2)the rates of biogeochemical reactions (Smith and Dukes 2013, Shepherd 2003, Hartley et al 2021, Romeo et al 2015) 3) the hydrological cycle, determining the clouds formation, the precipitation occurrence and the extent of snow and ice cover (Barnett et al. 2005, Kleidon and Renner 2013, Beniston et al.2014, Beniston et al. 2018).

The World Meteorological Congress has recognized the vital contribution of long-term weather observations in preserving our scientific memory and monitoring climate change, given the need for reliable historical records of the past to understand the present and prepare for the future. Currently, only 246 high-quality time series data of meteorological observations, spanning over decades or even centuries, allow scientists to study and understand the Earth's climate, including its variations and trends (WMO 2022). There is limited availability of long-term, homogeneous and comparable ground-based observations in most mountainous regions outside Western Europe and North America (Viviroli et al 2011). The Global Historical Climatology Network dataset (GHCN V.4) includes 27,467 meteorological stations, of which only 1328 (4.8%) are located above 2000 m asl and 211 (0.8%) are located above 3000 m a.s.l. The density of meteorological stations declines sharply above 3000 m a.s.l., and the GHCN dataset does not feature a single station located above 5000 m (Menne et al 2018). The lack of data from high elevations often leads to the use of data from lowland sites to evaluate processes in high mountain environments, resulting in uncertainties and poor characterization and modeling of high-elevation environments (Shahgedanova et al. 2021, Lundquist et al 2008). In mountainous environments, scientists have to deal with the inaccessibility and inhospitality of steep slopes, the complexity, diversity, and spatiotemporal variability of physical processes (e.g. the complex rugged topography), and the limited financial resources (Thornton, et al.2021). High elevation temperature can be monitored using remote sensing techniques, particularly through satellite-derived land surface temperature (LST)., because there is a strong relationship between air and surface temperature, but the low temporal resolution, the influence of surface emissivity, the presence of snow and cloud cover and the mismatch between satellites pixels and ground measurements can introduce uncertainties and biases. (Mo et al. 2025)The focus of the present study is on the calculation of a temperature time series at the highest meteorological stations of Switzerland. High elevation sites have many distinctive characteristics compared to the low-elevated one, they occupy about one quarter of the Earth's land surface and are home to nearly 20% of the world's population (Alfthan et al 2018). Mountains are the storehouse of biological diversity and endangered species, supporting about 25% of the terrestrial biodiversity and hosting 32% of the protected areas worldwide (Sayre et al. 2020). They provide essential resources such as water, food, energy and timber to over half of the global population, acting as the foundation for downstream communities. Mountains act as a major store of freshwater (Barnett et al., 2005; Viviroli et al., 2011), much of it currently in solid form (snow and ice). They hold intrinsic spiritual value due to their aesthetic appeal, recreational opportunities, tourism potential and the cultural heritage of the indigenous populations (UNESCO World Heritage List 2024). Despite their unique and pivotal role in human life and natural cycles, mountains and high elevations are considered a “climatic hotspot”. They experience greater warming rates than the rest of the globe, and the impacts of this warming are amplified due to the critical role that these areas play in the global climate system (Palazzi et al. 2019). Mountains are particularly sensitive to future changes in climate with numerous potential impacts ranging from decreasing biodiversity (La Sorte & Jetz, 2010), shrinking habitats for many species (Meza-Joya et al 2023, Loik 2024), mismatches between ecosystem components due to variable range shifts (Zu et al., 2021), declining snowpacks (Blau et al. 2024,carrer et al 2023), and retreating glaciers (Huss 2024, Pelto 2020, Hugonnet et al 2021, Huss & Hock, 2018; Zemp et al., 2019). The decline of the cryosphere has many consequences, including the potential loss of water supply for billions of people in downstream regions worldwide (Bradley et al., 2006; Viviroli et al., 2020) and the shifting of snowmelt from spring/summer to earlier in the year (Musselman et al., 2017). In regions where annual mean temperatures are presently close to the melting point, small shifts in temperature often have large hydrological consequences (Haeberli & Weingartner, 2020, IPCC 2019).

Within the Swiss territory, due to the high quality of the meteorological station network (characterized by high spatial resolution and standardized, homogenized daily temperature time series) many studies have aimed to create a gridded dataset covering the whole territory. MeteoSwiss has provided a dataset for the period 1961-2020 (MeteoSwiss Spatial Climate Analyses, 2021), and Isotta et al 2019 published a long-term consistent monthly temperature grid data set over the past 150 years. Pfister et al. (2020) provided a continuous spatial weather reconstruction for daily precipitation and temperature since 1864 (grid space of 2.2 km), using an analogue resampling method (ARM) based on station data and a weather type classification. An ensemble Kalman fitting approach and a quantile mapping were then applied in post processing (https://doi.pangaea.de/10.1594/PANGAEA.907579). This dataset was then extended by Imfeld et al. (2023), resulting in a 258-year daily temperature and precipitation dataset for Switzerland from 1763 to 2020 with a grid resolution of 1 km (Imfeld et al. 2023). In the broader Alpine region, spanning from 4° to 19°E and from 43° to 46°N, mean monthly temperatures (for different topographic heights) on a regular grid of 5 min grid-distance were estimated by Chimani et al. (2013). The gridded data is currently available at: https://www.zamg.ac.at/histalp, covering the period 1780-2014, obtained by merging high resolution climate mean grids (1961-1990) for each month and long term monthly station data. These two gridded databases will be used as a comparison to validate our long-term time series reconstruction.

This study focuses on reconstructing daily maximum, mean and minimum temperature time series from 1900 at the Jungfraujoch (Switzerland), the highest meteorological station within the Swiss territory and the reference of the ICOS network about the greenhouse gases monitoring (Cristofanelli et al 2023). Within the Aletsch UNESCO World Heritage Site, where the cryospheric components are pivotal factors for many environmental and biological processes, the peculiarity of its location makes the reconstruction of the daily temperature a reference for a backward simulation.

Key aspects of this work are: i) Define a low-data requirement method to reconstruct daily temperature at high elevation sites which can be easily extended at many other inaccessible sites over the world; ii) Estimate an historical time series which is temporally reliable; iii) The elevation dependent warming is an open issue and the evolution of the climate change remains unknown, that’s why is necessary to remove trends and estimating the model’s parameters on stationary dataset; ; iv) Evaluate the model performances in terms of correlation biases, autocorrelation and efficiency to select the right stations which provide reliable estimation at the target site; v) To ensure the quality of the estimated time series also in the period 1900-1933, a final comparison with Histalp and Imfeld gridded datasets will be presented, demonstrating comparable performances;vi) the reconstruction of the daily temperature from 1/1/1900 allows the comparison with others 7 uninterrupted time series measured at elevation above 1000 m

In the next, data descriptions and preliminary analysis are given in Section 2, Methods in Section 3, Results in Section 4, Discussion and Conclusions in Section 5.

2. DATA DESCRIPTION AND PRELIMINARY ANALYSIS

The Jungfraujoch is a High-Altitude Research Station (HFSJ) located in the saddle between the Jungfrau and Monch peaks in the Bernese Alps, on the boundary between the cantons of Valais and Bern, at the meteorological divide between North and South, at an altitude of 3500 m a.s.l. This site is considered as a mailstone for monitoring meteorological variables using standardised automatic sensors from 1980 and also provides unique visual weather observations of cloud type and height as well as precipitation thanks to the permanent presence of researchers. The shortwave solar radiation and long-wave thermal infrared are measured to study the effect of greenhouse gases on the infrared radiation emitted by the atmosphere to the ground and in the context of the ozone depletion problem. The Jungfraujoch is one of the stations in the National Air Pollution Monitoring Network (NABEL) operated by Empa and the Federal Office for the Environment (FOEN) and it is the highest measurement station within the ICOS network (https://www.icos-cp.eu), measuring carbon monoxide and dioxide, methane, nitrous oxide (Cristofanelli et al. 2023). Its altitude, its distance from any sources of pollutants and its very dry alpine air makes the Jungfraujoch especially suited for monitoring the column integrated gases concentrations (vertical profile) and the aerosols. The fine suspended particles, depending on their physical and chemical properties, change the characteristics of the clouds and affect the formation of ice in high altitude cirrus clouds (CLACE experiment). Secondary cosmic rays and radioactivity are monitored by two standardized neutron monitors to determine the primary cosmic ray flux and it energy spectrum (RADAIR network).It is well suited for long-term ground-based monitoring of the free troposphere because it is permanently manned and undisturbed measurements started in 1937 (Appenzeller et al 2008). It became automated in 1980. The MeteoSwiss database provides the daily maximum, minimum and mean temperature observations for the period 1961 to 2023 (from 1933 for the mean). Within this database, we selected daily temperature observations of the mean and extremes observed at 30 meteorological stations, sorting them according to the elevation and with uninterrupted measurements at least from the year 1971. In the following sections, the Jungfraujoch (JUN) will be named as the Target Site (TS) and the other 30 considered stations as the “back-up” stations (BS). MeteoSwiss provides a reliable and verified dataset, where every published value is accompanied with quality and mutation parameters flag, which describe suspected, missed or inconsistent data. For each station, Table S1 shows name, Latitude, Longitude, Elevation, Exposition, Distance from the target site; frequency distribution with the elevation, along with a geographic plot showing the respective location (Figure 1). 42% of these stations are below 1000 m a.s.l., 42% in the range from 1000 m to 2000 m a.s.l., while 16% are above 2000 m a.s.l. (Figure S3 a). 18 of 31 stations are inserted in the Swiss Basic Climatological Network (Swiss NBCN), where systematic measurements of climate parameters have been conducted since 1864. To increase the numbers of stations above 2700 m a.s.l., we included also: i) the Zugspitze monitoring observatory (DLZUG), part of the Germany National Meteorological Service (DWD) operational network, located at 2962 m a.s.l. on the Germany/Austrian border, 247 km from the Jungfraujoch site; ii) The Sonnblick observatory (SON), in the middle of the Eastern Austrian Alps and part of the Austrian national meteorological service (ZAMG) operational network, above an isolated peak at 3105 m a.s.l., 382 km from our target site.

The 30 MeteoSwiss "BS" stations are reported with light blue dots in Figure 1 along with the three other aforementioned historical observatory: Jungfraujoch (JUN, Red triangle), Sonnblick (SON, blue triangle), Zugspitze (DLZUG, green triangle). As one of the main purposes of this work is to provide a long-term daily consistent and reliable mean daily temperature at the target site, which started its observations in 1933, we turned to the HISTALP gridded dataset for monthly temperature data, which covers the period from 1780 to 2014 (Auer et al. 2007, Chimani et al. 2013 https://www.zamg.ac.at/histalp/datasets.php). Within this dataset, we selected the closest grid point to the JUN peak and we compared the mean monthly temperature time series with the observations (mean monthly values in the period 1933-2014), finding a bias of -2.05°C, likely due to the altitudinal gradient. In 2023 Imfeld et al. estimated the daily mean temperature time series for Switzerland on a 1 km grid. This high spatial resolution allowed to select the closest grid point characterized with a median bias (compared to daily observations at our target site in the period 1933-2020) equal to -0.13°C. These two historical time series (after bias correction) will be used as references to compare our estimated time series especially in the in the period 1900-1933 for a further validation. The comparison of mean annual error bars between the observations and unbiased time series from the aforementioned datasets (Figure S1) shows good agreement within the period 1940-1980. We highlight some discrepancies: before the year 1940, in the year 1981 and within the period 2005-2014. Some of these discrepancies can be related to: the introduction of automated measurements (1981), change of instrument type (1982), and instrumental problems (1992 to 1994), which characterized the history of the target meteorological station (Appenzeller et al. 2008). A positive trend in the mean annual temperature is also clear after the year 1970, reaching the cumulative value of +2.01°C by the end of 2023 (based on the cumulative moving average of monthly mean annual trends).

3. METHODS

Working with long-term daily temperature time series observed in mountain regions presents several challenges, including lack of data, temporal inconsistency (relocation, damage), and varying trends (sometimes nonlinear nor monotonic with elevation, latitude and longitude). To address these issues, we propose a methodology articulated in the following five steps (see also Figure S2):

Step 1: Data collection and preliminary analysis. Initially, daily observations of maximum, mean, and minimum temperatures from each meteorological station were retrieved, considering the entire period of observation (which is different among the BS stations as reported in the Table S1). We removed daily observations before a lack of data period greater than 30 days and we treated missed, suspicious and inconsistent data as “Not a Number” (under the definition by MeteoSwiss), defining a temporally consistent time series.

Step 2: Trend removal. Focusing on the period 1971-2023, we applied a detrending algorithm based on singular spectrum analysis (SSA, Elsner & Tsonis, 2013) to estimate and remove the mean monthly annual temperature trend from each BS record. The application of SSA does not require any a priori assumption on the trend’s shape (monotonic and linear trend are conventionally used in literature). After this passage, we performed Mann-Kendall and Cox Stuart statistical tests (with 0.05 significance level) to verify that the detrended time series were made stationary. The last test concerned the autocorrelation function stationarity, to exclude the occurrence of oscillatory components within the detrended time series. (Zhivomirov 2024). For each detrended time series, we calculated the annual values of standard deviation, asymmetry and kurtosis coefficients, and we applied the Mann-Kendall test, verifying that in most cases, the stationarity was reached for all three variables (max, mean and min). (In Section “Results”, we will explain in detail the comparison among the different trends which were found and the results of the Mann Kendall test on stationarity). The detrending procedure is critical, because the model’s parameters must be estimated using pairs of stations which are stationary, without the “anthropogenic” warming trend. Within the observation interval 1971-2023, where we can account on 30 BSs stations with daily consistent observation of minimum, mean, and maximum temperature, we distinguished three sub-intervals: the middle period 1988-2005, used as the calibration dataset to construct our model; the remaining intervals (1971-1987 and 2006-2023) to be used for validation purposes.

Step 3: Temperature estimation at target site. he daily temperature at the target site TS is calculated as follows:

$$T_{TS|BS,mod}(t) = T_{BS,obs}(t) + TLR_{BS,m}(Z_{TS} - Z_{BS}) + \varepsilon_{BS,m}(t) \tag{1}$$

where $T_{TS|BS,mod}$, is the temperature at TS calculated from the temperature at BS station, $T_{BS,obs}$; $TLR_{BS,m}(Z_{TS} - Z_{BS})$ is a deterministic component, the product of the temperature lapse rate $TLR_{BS,m}$ and the elevation difference between TS and BS, $(Z_{TS} - Z_{BS})$; $\varepsilon_{BS,m}$ is the residual, assumed a random noise.

The subscript "m" refers to the monthly variability of the parameters which is mandatory to follow the seasonal evolution of temperature, while the subscript "mod" means modelled.

The TLR is a key parameter in the atmospheric sciences, because it determines the stability of an air mass (https://www.rmets.org/metmatters/when-air-stable-or-unstable). This parameter varies from about -0.98°C/100m for dry air (i.e., the dry-air adiabatic lapse rate) to about -0.4°C/100 m (i.e., the saturated adiabatic lapse rate) (Rolland 2003). However, the process is rarely adiabatic and many factors can influence its temporal and spatial variability (water vapor, saturation, cloud cover, land cover, wind conditions, weather pattern). As an overall mean value over the world, the International Civil Aviation Organization (ICAO) defines an international standard atmosphere with no moisture with a temperature gradient equal to -6.5°C/km.

Calibration (1987-2005)

For each couple of TS and BS, within the calibration period, the TLR parameter was estimated, defining a possible range of variability from -1 to +1°C/100 m and calculating the sum of squared errors between observations and simulations. The optimal value of the TLR is that which minimizes the sum of squared errors. The difference between the observed time series and the deterministic component defines the residuals:

$$\varepsilon_{BS,m}(t) = T_{TS,obs}(t) - T_{BS,obs}(t) - TLR_{BS,m}(Z_{TS} - Z_{BS}) \qquad (2)$$

For each month, with the maximum likelihood method, the parameters of four statistical distributions (Normal, GEV, Stable, TLocationScale) were estimated. Kolmogorov Smirnov and Anderson Darling tests at 5% of significance level were applied to confirm or discard each distribution and the comparison among their lowest values suggested the best distribution. The calibration phase, for each couple BS-TS defines 12 values of the TLR, and depending on the best statistical distribution, from 24 to 48 parameters for the residual component.

Step 4: Performance evaluation. A particular effort was made to evaluate the model's performances in both calibration and validation periods. To this aim a set of indexes were calculated comparing the observed (obs) and modeled temperatures (mod): to evaluate the correlation, (1) the Pearson correlation coefficient ρ_P, (2) the Spearman's rho ρ_S, (3) the Kendall's tau τ_K; about biases (1) the mean bias b, (2) the root mean square error RMSE, (3) its normalized error (NRMSE), (4) the Klimt-Gupta efficiency (KGE). In the Supplementary materials, we provide the formulas to make their sample estimates.

Temperature reconstruction (1971-2023)

After the calibration phase, which consists of estimating the TLR and statistical distribution parameters of the residuals, for each meteorological stations, under the hypothesis of temporal invariance of the same coefficients we estimated the daily values of minimum, mean and maximum temperature within the period 1971-2023 using Eq.(1). The deterministic component will be the product of $TLR_{BS,m}(Z_{TS} - Z_{BS})$, and the residuals are the median of 1000 quantiles randomly extracted from the distribution of monthly residuals fitted in the calibration phase (Figure S14). We can compare each estimation of the temperature at the target site using separately each lower altitude station (one of the 32) by calculating the performance indexes (correlation coefficients, KGE and so on), both in calibration and in validation modes. In this way, we provided 32 different estimations of daily temperature at the target site.

Step 5: Stations selection. We then selected a subsample of the stations (n_{ens}) based on the KGE coefficient (greater than 0.9) to define a reliable time series, avoiding dependence on any single station that might fail or be damaged by harsh mountain conditions. The ensemble simulation was defined as the weighted mean of the KGE-based selected stations:

$$T_{TS,Ens}(t) = \sum_{i=1}^{n_{ens}} w_i T_{TS|BS_i,mod}(t) \tag{3}$$

where w_i is the normalized weight, properly defined accordingly to the KGE, related to each station:

$$w_i = \frac{KGE_i}{\sum_i^{n_{ens}} KGE_i} \tag{4}$$

where

$$KGE_i = 1 - \sqrt{(1-\rho_P)^2 + \left(1 - \frac{\mu(T_{TS|BS,mod})}{\mu(T_{TSobs})}\right)^2 + \left(1 - \frac{\sigma(T_{TS|BS,mod})}{\sigma(T_{TSobs})}\right)^2} \tag{5}$$

The ensemble simulation was then tested against the observations, under the evaluation of the same performance indexes previously defined (and reported on the Supplementary materials), which allows to compare the ensemble simulation with the pairwise one. Because we are interested in long-term daily temperature reconstruction, we did a backward simulation of the mean daily temperature time series which started in the year 1900.

An additional check to assess the reliability of the calculated ensemble we made a comparison with two independent datasets: Histalp and Imfeld et al. (2023). We selected the grid points of the two datasets closest to our target site and we compared the data with our TS temperature reconstruction. Within the periods 1933-2014 and 1933-2020, we estimated respectively a bias of -2.05°C for the Histalp time series and -0.13°C for the one of Imfeld et al. (2023). We removed these biases to define two temporally consistent and unbiased time series at the Jungfraujoch, which were then used to validate our ensemble simulation especially over the period 1900-1933, where observations were not available.

In the next section, the results of each of the previously presented steps will be explained in detail.

4. RESULTS

Starting from the analysis of the long-term temperature daily observations at each meteorological stations we will then proceed to reconstruct the daily temperature time series using the KGE-based weighted mean from the year 1900. The following subsection will mirror the flow chart phases (Figure S2) explaining in detail the results of each of them.

4.1 Time series observation analysis

4.1.1 1900-2023

The temporal consistency is a pivotal factor in the context of estimating reliable daily temperature time series and it is of even greater importance in a complex mountainous terrain such as Switzerland.

The harsh meteorological conditions and the distance from major cities or human settlements are the main obstacles to the continuity of daily values. Daily temperature observations time series provided by MeteoSwiss have already been pre-processed and a deep quality check control is a prerequisite before the publication on the Idaweb platform, so the only two processes we applied to the data are the classification as “Not a Number” of suspicious values and the removal of the part of the series before a lack of data greater than 30 days. About the maximum daily temperature at least 5 stations provided observations from the year 1900, 8 stations provided the minimum, and 15 the mean (see Figure S3 panel a). Within the period 1971-2023, 32 meteorological stations (called BS stations in the following sections), including the historical observatories of Sonnblick and Zugspitze as well as the Target Site at the Jungfraujoch, provided reliable daily temperature time series for the mean and extreme temperature values (Figure 1). This is why the calibration and validation of the models developed to reconstruct daily temperature at TS refer to this time interval. . First of all, we computed the time series of the first four empirical statistical moments (mean, standard deviation, coefficient asymmetry and kurtosis), for each year in the period 1900-2023 (Figure 2, S4, S5). We found a clear increasing trend in mean daily temperatures, especially marked after the year 1970, at all the sites considered. The annual mean and standard deviation are correlated together and strongly depend on the elevation with lower values which pertain to mountain peaks. The coefficient of asymmetry shows a generally negative value, with a left skewed statistical distribution typical of European mountain sites (Gubler et al 2023), where low values determine the heavy left tail. The annual values of the kurtosis coefficient are almost always lower than 3, which describes a platykurtic distribution. From this analysis, we can clearly say that the temperature statistical distribution is far from the gaussian distribution, because of the heavy tails which moves the asymmetry and kurtosis far from the 0 and 3 values respectively. There is a clear pattern with the elevation: mean, standard deviation, and kurtosis are lower at high elevation sites, and the opposite behavior characterizes the coefficient of asymmetry (Figure 2).

In a climatological context, it is important to analyze the annual anomalies of the statistical moments to determine if and how climate change affects the statistical distributions. Considering as reference period 1900-2023, 15 meteorological stations show a clear increasing trend of the annual mean, a periodical oscillation near the 0 about the annual standard deviation, a positive anomaly of the asymmetry coefficient after the 1970, and a clear reduction of the kurtosis coefficient from the 1960s (Figure S6).

4.1.2 1971-2023

Based on the temporal consistency analysis, we focus on the period 1971-2023 for the model calibration and validation phase. Because of the recent accelerating increasing trend on the mean daily temperature, we estimated the non-linear trend on the monthly mean time series for each station using the SSA algorithm (Chapter 3). The estimated cumulative annual temperature trend among the 33 meteorological stations are from -0.08°C to +2.4°C, +1.17°C to 2.5°C, and +0.19°C to 3.20°C, respectively for minimum, mean and maximum temperature. On 26/33 cases the annual daily thermal excursion increased due to the highest increasing rates of maximum temperatures (Table S2). The annual trend rate seems to be almost linear hiding the very high monthly variability. We did not find any clear pattern with the elevation, but we highlight the presence of just 7 values above 2000 m and a cluster of 22 below 1500 m a.s.l., and a more representative sample at high elevations are required to obtain more reliable results (Figure 3). The Elevation-Dependent Warming is an open issue and their investigation is on the frontier of the research, driven by the current greenhouse gases concentrations and their vertical profile (Pepin et al. 2022).

Time series modelling must account for autocorrelation between subsequent values, and the temperature is worldwide affected by the persistence property. Analyzing the autocorrelation function (50 days of lag) within the period 1971-2023, we found a clear trend with the stations' elevations: the lower altitude sites (light grey lines) are characterized by higher temporal correlation coefficients compared to the higher elevation ones (black lines and historical observatories) (Figure S8). The autocorrelation is another way to see the effect of the heatwaves' phenomena within cities and the cold air pool winter phenomena which drives the high autocorrelation coefficients, rather than the high exposure of the peaks and crest of the mountains, which favors the abrupt changing of the meteorological conditions. The negative vertical profile of the water vapour concentration in the atmosphere and the higher mountain clear sky view decreases the temporal autocorrelation of the temperature at high elevations.

The anomalies on the annual values of mean, standard deviation, coefficient of asymmetry and kurtosis were finally analyzed (the anomalies are defined as the difference between the current annual value and the mean of the period 1971-2023). The four subplots in the Figure S7 show the clear increasing trend rates of the mean annual anomalies about the mean and extremes temperature and also about the daily thermal excursion. We highlight that the variability among the 33 sites (30 BS stations plus the three historical observatories) were higher before the year 1981, when there was a transition between manual and automatic sensors. The similar behavior among stations is higher in terms of the mean temperature, while the extremes are generally affected by a higher variability. Despite the large distances and the difference in data source, the historical observatories of Zugspitze (blue lines) and Sonnblick (green lines) confirmed the same trends, emphasizing that elevation represents a key driver for temperature anomalies and about the correlation between long-term temperature time series. The anomaly checking also allows to evaluate the temporal consistency of the single station time series and to detect some derivatives on the monitoring instruments. The Jungfraujoch (red lines) anomalies about the maximum temperature and DTR (Daily Temperature Range: $T_{Max} - T_{Min}$) showed very lower values before the year 1990 compared against the other sites with the high spike in the year 1981 when the thermometer relocation occurred. Figure S9 shows the anomalies of the mean, standard deviation, skewness and kurtosis statistical moments: we found a clear positive trend about the mean, a slight positive trend on the standard deviation, an almost stationary time serie anomalies of the asymmetry and more pronounced negative trend on the kurtosis coefficient.

The different trend rates which affect maximum and minimum temperature suggest a need to evaluate the daily temperature excursion variability with the elevation. The lower panel of Figure S10 shows that there is a negative trend with the elevation, determined by the higher increase of maximum temperatures compared to the minimum ones especially at low elevation sites.

4.2 Model's parameters

After removing the trend for each temperature time series, we focused on the period 1988-2005 to estimate, for each pairwise BS-TS, the $TLR_{BS,m}$ monthly parameter (deterministic component) and the distribution of residuals (F($\varepsilon_{BS,m}$)).

4.2.1 Temperature Lapse Rate (TLR)

In the next, when we compare TLR monthly values we will refer to its absolute value.

Monthly values of the TLR parameters reflect the temperature seasonality, with a typical "U" shape. The estimated lower values pertain to winter months and higher ones to the summer season. The median values (among the 30 BS-TS pairwise) are from -0.43 to -0.59, -0.42 to -0.65, -0.45 to -0.74 (°C/100m) about min, mean and max temperatures (Table 1 and Figure 4 Panel a).

About the mean temperature, the highest median value was found in June (-0.651) and the lowest in December (-0.42), and the "U" shape in this case is evident. The max temperature shows the same trend with the exception of June, where the value is lower compared to May and July (M:-0.744, J:-0.657;J:-0.722). About the min temperature TLR is higher in April (-0.585) and lower in December (-0.427). In this latter case, we clearly see the effect of the thermal inversion phenomena (stagnation of cold pools air in the winter months on the valley stations); and the influence of warming created by the high water vapor content which smooths the excursion between winter and summer months (especially near water bodies).

The persistence of atmospheric stability conditions in summer months determines the higher values of the TLR of maximum temperature, where the dry air, clear sky and the high solar radiation increase the elevation gradient. The boxplot interquartile range and whiskers show the higher variability of the maximum temperature compared to the minimum ones, which are more concentrated near the median values. Within Figure 4 we plotted with dashed red lines the Mean Environmental Lapse rate (0.65°C/100m) and the dry adiabatic Lapse Rate of 0.98°C/100m for comparison.

4.2.2 Statistical Distributions of residuals

As we have seen from the analysis of the statistical moments of the observed time series (Figure 2), the annual distribution of the daily temperature time series is far from the normality, with negative skewed asymmetric distributions and platykurtic kurtosis coefficients. The fitting of the residuals statistical distributions suggested the same behavior, because the Generalized Extreme Value distribution is, in 30/36 of the cases, the one having the lower values of KS (Kolmogorov-Smirnov) and AD (Anderson-Darling) statistics (Figure 4 Panel b). This means that the heavy tails affect the distribution of residuals and that the normal distribution is never the best one among the four considered. We have to highlight that the distribution considered here is the mode among the 30 pairwise of BS-TS.

TLR and distributions of residuals and their parameters, with monthly variability, are fitted in the calibration period and then preserved to simulate the whole time series in the period 1900-2023.

4.3 Model Performances

The observation period from 1971-2023 common at all of the 30 stations, allowed to define the 1988-2005 as the calibration period, and use the previous and the following periods to validate the models' performances. First, we analyzed the pairwise performances which have been obtained with the comparison between the estimated (see equation 1) and the observed time series at the Jungfraujoch target site. In the following Figures and Tables, we will report just Cal and Val terms to simplify the visualization: with "Cal" we will indicate the 1988-2005 period and with "Val" the overall 1971-2023.

Four performance indexes (NRMSE, BIAS, KGE and ρ_{Sp}) help to quantify the performance variability among the different stations (30 in Swiss + ZUG and SON), about the min, mean and max temperatures (Figure 5). To the mean temperature pertain lowest bias values (Cal=0.063°C and Val=0.121°C), lowest NRMSE (Cal=0.474 and Val=0.470), highest KGE (Cal=0.874 and Val=0.866), highest Spearman's correlation coefficients (Cal=0.896, Val=0.895) and lowest IQR ranges. We found a negative bias on the max temperature in the Validation period which is correlated with high temperature anomalies within the observation in the last 4 years (2020-2023). The comparison between validation and calibration periods shows the same performance levels. The ensemble simulation performances about the mean temperature in the calibration/validation periods are 0.286/0.286, 0.077/0.106, 0.949/0.941, 0.963/0.964 respectively for NRMSE, Median Bias, KGE and ρ_{SP} suggesting that the ensemble's performances are at the upper bound of the correlation coefficients and at the lower bound about the errors. Table S3 shows the individual stations' performances for all the 3 variables. The pairwise models' performances were evaluated also in relation to the stations' characteristics: distance, elevation, latitude, longitude, aspect. We found that the elevation plays a pivotal role by increasing the correlation and decreasing the errors among each BS stations and the target site TS (see the clear trends of NRSME, KGE, ρ_{SP} and τ_K in Figure S11). Just the median bias values seem to not be affected by the elevation.

The time series estimation must be evaluated also in terms of its autocorrelation structure, especially when a daily time scale was considered. The results suggest that also in this case the highest altitude station preserve the same autocorrelation function compared to the low valley ones. The key message here is that the elevation difference between TS and BS has a reverse proportion with the model performances. The ensemble simulation performs well also in this context especially when we consider the mean and max temperatures (Figure S12 Panel a). Because the ensemble was defined as a weighted mean of many stations, intrinsically, by definition, its autocorrelation increases compared to the original variables. Finally, we evaluated the annual anomalies (Figure S12 Panel b).

The median annual biases of the ensemble min, mean and max temperature are: 0.32, 0.22, -0.05°C, but we can see very high spikes in maximum temperature focused on the years: 1981 (+1.90°C), 1991 (+0.89°C), 1995 (+0.96°C), 2022 (-1.11°C). Since high spikes are present in all BS stations, we hypothesize that the cause lies within the TS observed time series, which was subjected to shift inhomogeneities in the years 1981,82,92,94 as reported in Appenzeller et al. 2008).

Related to the maximum temperature, we found high negative biases in the last 4 years (2020-2023) with a maximum value equal to -1.11°C; that is why we think that the ensemble is a good tool to detect the anomalies and shows the direction future studies must take.

The comparison between the ensemble simulation and the observations' daily error bar is shown in Figure 6, where panels a and b respectively refer to daily and annual scales.

The ensemble has high KGE coefficient values, always greater than 0.932 both in calibration and validation periods. Focusing on panel a and validation period we found a slight underestimation of min and mean temperature in winter and summer months rather than the maximum which are overestimated especially from June to September.

The annual error bar (panel b) suggests a very good agreement about the mean temperature but a slight underestimation in the upper bound of the error bar related to the minimum temperature and some discrepancies in the years 1981, 2005, 2022 about the maximum temperature.

4.4 Long-term time series reconstruction

Here, we will present a comparison between the ensemble simulation and the observation of the daily mean temperature available from the year 1933 (Table 2). We also compare the annual anomalies with estimates from the closest grid point of the Histalp gridded dataset for the period 1900–2014 and from the daily gridded dataset provided by Imfeld et al. (2023) for the period 1900–2020. The latter two datasets were previously corrected for a constant bias.

Figure 7 illustrates the comparison between the modeled and observed time series both at daily scale (panels a, b and c), and annual scale (panel d). We found a mean bias of 0.239°C mainly driven by the high anomalies before the year 1940, and an overall general slight underestimation on the rest of the simulation period. The Spearman correlation coefficient equal to 0.96 and the KGE greater than 0.93 confirm the high correlation, and the error bar shows that the mean daily value is reached well, but the boundary of the standard deviation range of the ensemble simulation is lower than the observed one (due to its definition as the mean of a number of stations which have residuals which are GEV-distributed). The autocorrelation structure is preserved but we found an overestimation because of the intrinsic definition of the ensemble (as the mean of many variables and generally the mean has and high autocorrelation compared to the original variable). Finally, the annual time series shows an overall good reliability of the model, with some periods which are affected by high errors (before 1938, in the period 1981-1985).

For further validation (Figure S13), we compared the ensemble simulation with the estimation published by Imfeld et al in 2023 at daily scale in the period 1900-1971 (we selected this period because we have already compared the performance with the observations over the period 1971-2023). In this period, we found a mean bias of 0.121°C but high correlation coefficient (0.956), with a light underestimation in January and February. Also, in this case the ensemble estimated a slower standard deviation compared to the Imfeld ones (Table 2). The comparison with this database suggests that the proposed methodology provides a reliable time series also in a backward analysis.

Finally, in panel d, we compared the annual time series anomalies among our estimation, those estimated within the Histalp project (cyan lines) and that obtained by Imfeld et al. (2023) (green lines), where dashed lines are referred to the unbiased time series. The statistics' anomalies of the ensemble simulation are very similar with the estimation published by Imfeld et al. (2023) (Table S4, Figure S13), and better compared to the Histalp one. The ensemble underestimated the mean annual temperature and the mean bias is equal to 0.25°C and higher positive anomalies were found in the period 1960-1970 compared to the other two. Before the year 1940 there was a general underestimation of the observed temperature which may be attributed to instrumental problems. Highest spikes can be observed in the years: 1963 (+0.92°C), 1981 (+1.06), 2005 (+0.79°C), with the latter two confirmed by Imfeld et al. (2023) and Histalp (Table S4 compares the anomalies statistics' also with the unbiased time series).

4.5 1900-2023 Anomalies Comparison

The 2024 observed global warming reaches the historic record of + 1.29°C above the 20th-century Earth's average land and ocean surface temperature (NOAA's 2024 annual global climate report), but the climate change hits each region differently, and the European Alps is considered a climatic hotspot. The reconstruction of the daily Temperature from 1900 to 1933 previously presented allows to compare the Jungfraujoch with other 7 historical time series of meteorological stations above 1000 m (Figure 8). Particularly we focused on annual anomalies (of the first two central statistical moments: the mean and the standard deviation), which was defined, for each site, as the difference between the annual mean (or the standard deviation) temperature with the annual mean of the period 1900-2023. To smooth the interannual variability we calculated the 10 years moving average, finding the same trend for all sites. About the Target site our estimation pointed out a rising temperature of +1.74°C at 2023, close to +1.87° C and +1.84° C of Sonnblick and Saentis and with an abrupt steep positive slope after the '80. The estimated anomalies fit well the Sonnblick mean Temperature annual anomalies even if the ensemble simulation doesn't consider this BS station because its KGE was less than 0.9. particularly the two time series overlap perfectly from 1900-1923, from 1941-1968 and from 1985-2008. This is remarkable because the two historical observatories are 383 Km far, and this is an ulterior confirmation that the elevation plays a key role in driving the rise of the temperature. We also highlight a very rapid increase of the mean temperature from 1940 to 1947 and a prolonged cooler-than-average period between 1951 to 1984 consistent for all the sites. About the standard deviation anomalies we found a very good agreement between ZUG and JUN before the year 1967 and from 1978-1990 and their values are generally comprised from -0.5 to 0.5 °C. From 1960 to 2020 there is an interesting sinusoidal shape (with an hypothetical period of 20 years) with positive peaks in the years: 1967-1984-2009 and negative ones in: 1976 and 1993. The mathematical definition of mean and standard deviation defines the correlation between them but when we consider the anomalies this correlation seems to be lost. The timeseries anomalies comparison among different sites is a good tool to detect instrumental derivatives or tipping points and their comparison with others meteorological variables helps to explain which are the possible driving factors.

5. DISCUSSION AND CONCLUSIONS

This work is motivated by the need to develop a temporally consistent statistical approach, low-data-requirement, for estimating daily temperatures at high elevations, addressing the gap in long-term daily temperature observations. To this end, we retrieved daily observations of mean and extremes daily temperature of the highest meteorological stations with continuous daily observation at least from 1971 from the quality-checked MeteoSwiss database. To increase the number of stations in the range 2600-3500 m a.s.l., we included the historical observatories of Sonnblick (3106 m) and Zugspitze (2904 m). Then we selected the highest meteorological station, Jungfraujoch, as target site, because it is a privileged site for monitoring the atmospheric conditions, greenhouse gases concentrations, air quality and cloud formation. A preprocessing phase consisted in the analysis of the statistical moments of the 33 daily temperature time series (max, mean and min) from 1900 to 2023, which highlight the steep increase of the mean annual temperature during the last 45 years.he trend's analysis shows a clear positive trend of 1.43°C, 1.81°C and 1.86 °C (min, mean, max) about the annual temperature and an increase in the daily thermal excursion equal to +0.41 °C. Trend rates and DTR are evaluated in relation to the elevation, but only about the latter we found a negative elevational trend equal to -0.31°C/km. The analysis revealed negative skewness and platykurtic features in the daily temperature distributions. The anomalies of the other three statistical moments (σ,β,γ) have a mean value of zero suggesting a more sophisticated variability. Focusing on the last 52 years, we removed the temperature trend of the mean monthly temperature of each site and we selected for model calibration and validation respectively the periods 1988-2005 and 1971-2023. Then we selected the highest meteorological station, Jungfraujoch, as the target sites and the others 32 as backup stations. The method of reconstructing the historical daily temperature time series at the target site is the weighted mean of several low altitude stations selected by a KGE coefficient greater than 0.9. The KGE coefficient is a commonly used index in hydrology, and here was adopted to evaluate the pairwise model performance during the calibration period. The pairwise (BS-TS) daily temperature estimations are defined as the sum of the observed temperature at each low altitude station plus a deterministic and stochastic component. The first is the product of the TLR and the altitudinal gradient and the second is a random extraction from the residuals' statistical distribution (TLR and residuals distribution are fitted comparing observation and estimation in the calibration period at monthly scale). The pairwise model performances were evaluated according to biases (mean, RMSE, NRMSE), correlation coefficients of Spearman, Kendall, Pearson, and the Klimt-Gupta Efficiency. We found comparable performances in both the calibration (1988-2005) and validation (1971-2023) periods suggesting the temporal invariance of the quality of the assessments and a clear pattern with the station elevations: higher stations' elevations perform better than the low altitude ones. This is a warning about the use of low altitude temperature time series in the estimation of high elevations sites. The former can be affected by very different local phenomena due to anthropogenic factors such as the heat island, or the cold air pool phenomena strongly decreasing the temperature correlation even if the two stations are very close together in terms of latitude and longitude. However, the use of weather stations at low altitudes is necessary since they have the longest observed time series, and a compromise between the length of the time series and the correlation must be reached.

The choice of using KGE > 0.9 as the criterion for selecting stations in the ensemble is open to discussion, but we opted for this index because it considers both the correlation and the first two statistical moments. It should be noted that sorting stations by elevation would yield similar results. The KGE-based weighted mean used to define the ensemble simulation is a key innovation of this study, offering several advantages:

i) it removes dependence on a single station observation, ii) it increases the estimations' temporal consistency and temporal autocorrelation, decreasing the influence of local phenomena; iii) it increases the reliability of the mean simulated value decreasing anomalies and biases. Comparing the ensemble simulation with the observations in the period 1971-2023 under the hypothesis of time-invariance of the TLR and residuals distribution parameters, we obtained good performances both over the calibration and validation periods, suggesting high correlation and low biases. The investigation of the best statistical distributions of the residuals is a novelty. We found that these residuals preserved the shape of the temperature distribution (asymmetric and platykurtic), which led to a fit with the Generalized Extreme Value (GEV) distribution, in contrast to the Gaussian normal distribution typically used. In addition to the mean daily temperature, we estimated also the extremes (max and min) because inside the Alpine Region they can behave differently under the influence of many natural and or anthropogenic factors (exposition to the solar radiation, atmospheric water vapor content, greenhouse gases concentration, aerosol, clouds) and they can be affected by differential altitudinal trends. To verify the reliability of this simple method, we compared the ensemble simulations with estimates from the closest grid point (at our target site) provided by Imfeld et al. (2023) and the Histalp project. The calculation of the annual mean temperature anomalies, correlation coefficients and biases confirmed that the ensemble simulations have a comparable reliability. The low data requirements of the presented methodology allows to extend the daily temperature long-term reconstruction at high elevations worldwide enhancing the possibility to study phenomena such as Elevation-Dependent Warming (EDW).

Open issues which need further investigation are: 1) modeling the dependence of higher order statistical moments (asymmetry and kurtosis) with the elevation, which could improve the performance of the proposed model 2) The shape of the residuals distribution suggests the need of a skewed statistical distribution as a skewed normal or a skewed exponential to better define the tails. In our method flow chart the temperature trend was removed, but if additional variables are measured, these latter can be introduced in the model.

The need of historical records of the temperature at high elevations suggest applying this method to other under-investigated mountain chains like Hymalaya or Andes mainly because they host a huge glacierized area with deep implication of the water supply of the lowlands populations.

SUPPORTING INFORMATIONS

Acronyms And Line-Box-Plot Styles Descriptions

In the optic of rendering fluently readable the main text, we're briefly describe the acronyms and figure line colors settings:

- "TS" is the target site of the Jungfraujoch, which has the identification code of "JUN" and an ID number of 101. The observed time series is generally plotted with Red Color;

- "BS" are the 30 lower elevation meteorological stations within Switzerland which have ID numbers from 301-330. Each observed time series have been generally plotted with greyscale color (Higher elevated stations tend to have darker style);
- "SON" and "DLZUG" are the Sonnblick and Zugspitze historical observatories, with ID number of 201 and 202 with green and blue bold lines colors;
- Within figures and graphs which show the comparison between the modeled and observed time series the first will be drowned with red color and the second with blue one.
- Minimum, mean and maximum temperature have respectively blue, green and red lines/dots styles;
- Error bar plot represents the mean plus/minus the standard deviation of the variable;
- Within the boxplots: The notch extremes correspond to $[q_2 - 1.57(q_3 - q_1)/\sqrt{n}\,]$ and $[q_2 + 1.57(q_3 - q_1)/\sqrt{n}]$, where q_2 is the median, q_1 and q_3 are the 25th and 75th percentiles. The rectangular box is delimited by q_3 and q_1;

Additional Figures and Tables

Within the Supplementary Material the readers can find:

- Figures from S1 to S13;
- Tables from S1 to S4;

All of them are cited at appropriate points in the main text of the manuscript, e.g. '(as shown in Figure S1)'.

AUTHOR CONTRIBUTIONS

Marco Bongio performed data analyses and made all the manuscript figures with advice from Riccardo Scotti, Giovanni Baccolo, and Carlo De Michele. The model's code was implemented by Marco Bongio in Matlab. Marco Bongio wrote the manuscript with contributions from all co-authors.

ACKNOWLEDGEMENTS

Many thanks to the two anonymous reviewers of the previous version for their precious suggestions on the manuscript improvements. We are sincerely grateful to Michela Buizza for her review about the manuscript's English language.

REFERENCES

Alfthan, B., Andresen, M., Gjerdi, H. L., Jurek, M., Puikkonen, L., Semernya, L., and Schoolmeester, T., 2018. Mountain Adaptation Outlook Series – Synthesis Report. United Nations Environment 26 Programme, and GRID-Arendal, Nairobi, Kenya, Vienna, Austria, and Arenda, Norway, 51 pp. ISBN 27 9788277011806.

Appenzeller, C., Begert, M., Zenklusen, E., & Scherrer, S. C. (2008). Monitoring climate at Jungfraujoch in the high Swiss Alpine region. *Science of the Total Environment*, *391*(2–3), 262–268. https://doi.org/10.1016/j.scitotenv.2007.10.005

Auer, I., R. Böhm, A. Jurkovic, W. Lipa, A. Orlik, R. Potzmann, W. Schöner, M. Ungersböck, C. Matulla, K. Briffa, et al. 2007. HISTALP—Historical instrumental climatological surface time series of the Greater Alpine Region. International Journal of Climatology 27:17–46. doi:10.1002/(ISSN)1097-0088.

Barnett, T., Adam, J., Lettenmaier, D. (2005). Potential impacts of a warming climate on water availability in snow-dominated regions. Nature 438, 303–309. https://doi.org/10.1038/nature04141

Beniston M., Stoffel M. (2014). Assessing the impacts of climatic change on mountain water resources, Sci. Total Environ., 493,1129-1137, https://doi.org/10.1016/j.scitotenv.2013.11.122

Beniston, M., Farinotti, D., Stoffel, M., Andreassen, L. M., Coppola, E., Eckert, N., Fantini, A., Giacona, F., Hauck, C., Huss, M., Huwald, H., Lehning, M., López-Moreno, J.-I., Magnusson, J., Marty, C., Morán-Tejéda, E., Morin, S., Naaim, M., Provenzale, A., Rabatel, A., Six, D., Stötter, J., Strasser, U., Terzago, S., and Vincent, C. (2018). The European mountain cryosphere: a review of its current state, trends, and future challenges, The Cryosphere, 12, 759–794, https://doi.org/10.5194/tc-12-759-2018

Blau, M. T., Kad, P., Turton, J. v., & Ha, K.-J. (2024). Uneven global retreat of persistent mountain snow cover alongside mountain warming from ERA5-land. Npj Climate and Atmospheric Science, 7(1), 278. https://doi.org/10.1038/s41612-024-00829-5

Bradley, R.S., M. Vuille, H.F. Diaz, and W. Vergara. 2006. Climate change. Threats to water supplies in the tropical Andes. Science 312: 1755–1756. https://doi.org/10.1126/science.1128087.

Carrer, M., Dibona, R., Prendin, A. L., & Brunetti, M. (2023). Recent waning snowpack in the Alps is unprecedented in the last six centuries. *Nature Climate Change*, *13*(2), 155–160. https://doi.org/10.1038/s41558-022-01575-3

Chimani, B., Matulla, C., Böhm, R. and Hofstätter, M. (2013), A new high resolution absolute temperature grid for the Greater Alpine Region back to 1780. Int. J. Climatol., 33: 2129-2141. https://doi.org/10.1002/joc.3574

Cristofanelli, P., Fratticioli, C., Hazan, L., Chariot, M., Couret, C., Gazetas, O., Kubistin, D., Laitinen, A., Leskinen, A., Laurila, T., Lindauer, M., Manca, G., Ramonet, M., Trisolino, P., Steinbacher, M. (2023). Identification of spikes in continuous ground-based in situ time series of CO2, CH4 and CO: an extended experiment within the European ICOS Atmosphere network, Atmos. Meas. Tech., 16, 5977–5994, https://doi.org/10.5194/amt-16-5977-2023.

Elsner, J.B., Tsonis, A.A., 2013. Singular Spectrum Analysis: A New Tool in Time Series Analysis. Springer, US, New York, USA.

H. V. Gupta, H. Klimt, K. K. Yilmaz, G. F. Martinez, (2009). Decomposition of the mean squared error and NSE performance criteria: Implications for improving hydrological modelling, Journal of Hydrology, V. 377, 80-91, https://doi.org/10.1016/j.jhydrol.2009.08.003.

Haeberli, W., & Weingartner, R. (2020). In full transition: Key impacts of vanishing mountain ice on water-security at local to global scales. *Water Security*, *11*. https://doi.org/10.1016/j.wasec.2020.100074

Hartley, I. P., Hill, T. C., Chadburn, S. E., & Hugelius, G. (2021). Temperature effects on carbon storage are controlled by soil stabilisation capacities. *Nature Communications*, *12*(1). https://doi.org/10.1038/s41467-021-27101-1

Hugonnet, R., et al., 2021: Accelerated global glacier mass loss in the early twenty-first century. Nature 592, 726–731. doi.org/10.1038/s41586-021-03436-z

Huss, M. & Hock, R. Global-scale hydrological response to future glacier mass loss. *Nat. Clim. Chang*. **8**, 135–140 (2018).

Huss, M. (2024). The Alps' iconic glaciers are melting, but there's still time to save the biggest. Bulletin of the Atomic Scientists, 80(4), 225–229. https://doi.org/10.1080/00963402.2024.2364501

IPCC (2019). IPCC Special Report on the Ocean and Cryosphere in a Changing Climate [H.-O. Pörtner, D.C. Roberts, V. Masson-Delmotte, P. Zhai, M. Tignor, E. Poloczanska, K. Mintenbeck, A. Alegría, M.

Imfeld, N., Pfister, L., Brugnara, Y., and Brönnimann, S. (2023). A 258-year-long data set of temperature and precipitation fields for Switzerland since 1763, Clim. Past, 19, 703–729, https://doi.org/10.5194/cp-19-703-2023.

Isotta, F. A., Begert, M., & Frei, C. (2019). Long-term consistent monthly temperature and precipitation grid data sets for Switzerland over the past 150 years. Journal of Geophysical Research: Atmospheres, 124, 3783–3799. https://doi.org/10.1029/2018JD029910

La Sorte FA, Jetz W. Projected range contractions of montane biodiversity under global warming. Proc Biol Sci. 2010 Nov 22;277(1699):3401-10. doi: 10.1098/rspb.2010.0612. Epub 2010 Jun 9. PMID: 20534610; PMCID: PMC2982223.

Loik, M. E. (2024). Press, pulse, and squeeze: Is climatic equilibrium ever possible on mountains? *Biological Conservation*, *291*. https://doi.org/10.1016/j.biocon.2024.110468

Lundquist JD, Pepin NC, Rochford C. 2008. Automated algorithm for mapping regions of cold-air pooling in complex terrain. Journal of Geophysical Research Atmospheres 113:D22107. https://doi.org/10.1029/2008jd009879.

Kleidon, A., Renner, M. (2013). A simple explanation for the sensitivity of the hydrologic cycle to surface temperature and solar radiation and its implications for global climate change, Earth Syst. Dynam., 4, 455–465, https://doi.org/10.5194/esd-4-455-2013.

Menne MJ, Williams CN, Gleason BE, Rennie JJ, Lawrimore JH. 2018. The Global Historical Climatology Network monthly temperature dataset, Version 4. Journal of Climate 31(24):9835–9854. https://doi.org/10.1175/JCLI-D-18-0094.1.

Meza-Joya, F. L., Morgan-Richards, M., Koot, E. M., & Trewick, S. A. (2023). Global warming leads to habitat loss and genetic erosion of alpine biodiversity. Journal of Biogeography, 50(5), 961–975. https://doi.org/10.1111/jbi.14590

Yaping Mo, Nick Pepin, Harold Lovell (2025). Understanding temperature variations in mountainous regions: The relationship between satellite-derived land surface temperature and in situ near-surface air temperature. Remote Sensing of Environment, volume 318, pages 114574, https://doi.org/10.1016/j.rse.2024.114574.

Musselman, K. N., Clark, M. P., Liu, C., Ikeda, K., & Rasmussen, R. (2017). Slower snowmelt in a warmer world. Nature Climate Change, 7(3), 214–219. https://doi.org/10.1038/nclimate3225

Palazzi, E., Mortarini, L., Terzago, S., & von Hardenberg, J. (2019). Elevation-Dependent-Warming in global climate model simulations at high spatial resolution. *Climate Dynamics*, *52*(5–6), 2685–2702. https://doi.org/10.1007/s00382-018-4287-z

Pelto, M., WGMS Network. (2020). Alpine glaciers [*State of the Climate in 2019*]. Bulletin of the American Meteorological Society, 101(8), S37–S38. doi.org/10.1175/2020BAMSStateoftheClimate.1.

Pepin, N. C., Arnone, E., Gobiet, A., Haslinger, K., Kotlarski, S., Notarnicola, C., et al. (2022). Climate changes and their elevational patterns in the mountains of the world. Reviews of Geophysics, 60, e2020RG000730. https://doi.org/10.1029/2020RG000730

Pfister, L., Brönnimann, S., Schwander, M., Isotta, F. A., Horton, P., & Rohr, C. (2020). Statistical reconstruction of daily precipitation and temperature fields in Switzerland back to 1864. Climate of the Past, 16(2), 663–678. https://doi.org/10.5194/cp-16-663-2020

Rolland, C. (2003). Spatial and Seasonal Variations of Air Temperature Lapse Rates in Alpine Regions. Journal of Climate 16(7) pp. 1032-1046. Available at: https://journals.ametsoc.org/view/journals/clim/16/7/1520-0442_2003_016_1032_sasvoa_2.0.co_2.xml [Accessed 10 Apr 2024]

Romeo, R., Vita, A., Mnauelli S., Zanini, E., Freppaz, M., Stanchi, S. (2015). Understanding Mountain Soils: A contribution from mountain areas to the International Year of Soils 2015.

Sayre R., Karagulle D., Frye C., Boucher T., Wolff N. H., S. Breyer S., D.Wright, M.Martin, K. Butler, K. Van Graafeiland, J. Touval, L. Sotomayor, J. McGowan, E.T. Game, H. Possingham, An assessment of the representation of ecosystems in global protected areas using new maps of World Climate Regions and World Ecosystems, Global Ecology and Conservation, Volume 21, 2020,https://doi.org/10.1016/j.gecco.2019.e00860.

Shahgedanova, M., Adler, C., Gebrekirstos, A., Grau, R.H., Huggel, C., Marchant, R., Pepin, N., Vanacker, V., Viviroli, D., and Vuille, M. (2021). Mountain observatories: status and prospects to enhance and connect a global community. Mt. Res. Dev.

Sheldon, K.S., Tewksbury, J.J. (2014). The impact of seasonality in temperature on thermal tolerance and elevational range size. Ecology, 95: 2134-2143. https://doi.org/10.1890/13-1703.1

Shepherd T. G. (2003). Large-Scale Atmospheric Dynamics for Atmospheric Chemists. Chemical Reviews 2003 103 (12), 4509-4532 https://doi.org/10.1021/cr020511z

Smith, N.G., Dukes, J.S. (2013). Plant respiration and photosynthesis in global-scale models: incorporating acclimation to temperature and CO2. Glob Change Biol, 19, 45-63. https://doi.org/10.1111/j.1365-2486.2012.02797 .

Viviroli, D., Kummu, M., Meybeck, M. *et al.*Increasing dependence of lowland populations on mountain water resources. *Nature Sustain*ability **3**, 917–928 (2020). https://doi.org/10.1038/s41893-020-0559-9

Viviroli, D., Archer, D. R., Buytaert, W., Fowler, H. J., Greenwood, G. B., Hamlet, A. F., Huang, Y., Koboltschnig, G., Litaor, M. I., López-Moreno, J. I., Lorentz, S., Schädler, B., Schreier, H., Schwaiger, K., Vuille, M., Woods, R. (2011). Climate change and mountain water resources: overview and recommendations for research, management and policy, Hydrol. Earth Syst. Sci., 15, 471–504, https://doi.org/10.5194/hess-15-471-2011.

World Meteorological Organization (2022). Centennial Observing Stations State of Recognition Report – 2021. Technical report, WMO-No. 1296, (2022). ISBN 978-92-63-11296-5, https://library.wmo.int/idurl/4/58048

World Meteorological Organization (2023) .Guide to Instruments and Methods of Observation Volume I – Measurement of Meteorological Variables WMO-No. 8, ISBN 978-92-63-10008-5, *https://library.wmo.int/idurl/4/68695*

Zemp, M., et al., 2019: Global and regional glacier mass changes from 1961 to 2016. (Version 1.1.0). doi.org/10.5281/zenodo.3557199

H. Zhivomirov (2024). Signal Stationarity Estimation with Matlab (https://www.mathworks.com/matlabcentral/fileexchange/75118-signal-stationarity-estimation-with-Matlab)

Zu, K., Wang, Z., Zhu, X., Lenoir, J., Shrestha, N., Lyu, T., Luo, A., Li, Y., Ji, C., Peng, S., Meng, J., & Zhou, J. (2021). Upward shift and elevational range contractions of subtropical mountain plants in response to climate change. *Science of the Total Environment*, *783*. https://doi.org/10.1016/j.scitotenv.2021.146896

Tables

TLR [°C/km]															
		Jan	**Feb**	**Mar**	**Apr**	**May**	**Jun**	**Jul**	**Aug**	**Sept**	**Oct**	**Nov**	**Dec**	Min	Max
T_{Min}	Med	-4.43	-4.84	-5.56	-5.85	-5.60	-5.71	-5.44	-5.29	-5.03	-4.72	-4.61	-4.27	-5.85	-4.27
	IQR	0.88	0.74	0.52	0.44	0.57	0.53	0.50	0.76	0.60	0.64	0.75	0.87	0.44	0.88
T_{Mean}	Med	-4.57	-5.12	-5.97	-6.37	-6.47	-6.51	-6.46	-6.30	-5.73	-5.16	-4.66	-4.20	-6.51	-4.20
	IQR	0.83	0.63	0.35	0.42	0.41	0.54	0.68	0.69	0.57	0.70	0.62	0.80	0.35	0.83
T_{Max}	Med	-4.96	-5.74	-6.66	-7.21	-7.44	-6.57	-7.22	-7.16	-6.38	-6.34	-5.22	-4.46	-7.44	-4.46
	IQR	1.01	0.78	0.73	0.50	0.67	0.61	0.82	0.91	0.80	1.11	0.84	0.98	0.50	1.11

Residual's Distribution Function (Mode of BS Stations)												
	Jan	**Feb**	**Mar**	**Apr**	**May**	**Jun**	**Jul**	**Aug**	**Sept**	**Oct**	**Nov**	**Dec**
T_{Min}	Gev	Gev	Gev	Gev	Stable	Gev	Gev	Stable	Gev	Gev	Gev	Gev
T_{Mean}	Gev	Gev	Gev	Gev	Stable	Tloc	Stable	Gev	Stable	Gev	Gev	Gev
T_{Max}	Gev	Gev	Gev	Gev	Gev	Gev	Gev	Gev	Gev	Gev	Gev	Gev

Table 1 Median and interquartile range of the TLR parameter for minimum, mean and maximum temperature and mode of the residuals' distribution function within the calibration period 1988-2005.

Ensemble Performances		
Index	**Vs Obs 1933-2023**	**Vs Imfeld (1900-2020)**
Bias [°C]	0.239	0.262
NRMSE	0.292	0.303
ρ_{Sp}	0.963	0.958
τ_K	0.832	0.821
KGE	0.935	0.928

Table 2. Ensemble Performances in comparison with Daily mean temperature observations in the period 1933-2023 and the estimated time series by Imfeld et al. (2023) within the period 1900-2020.

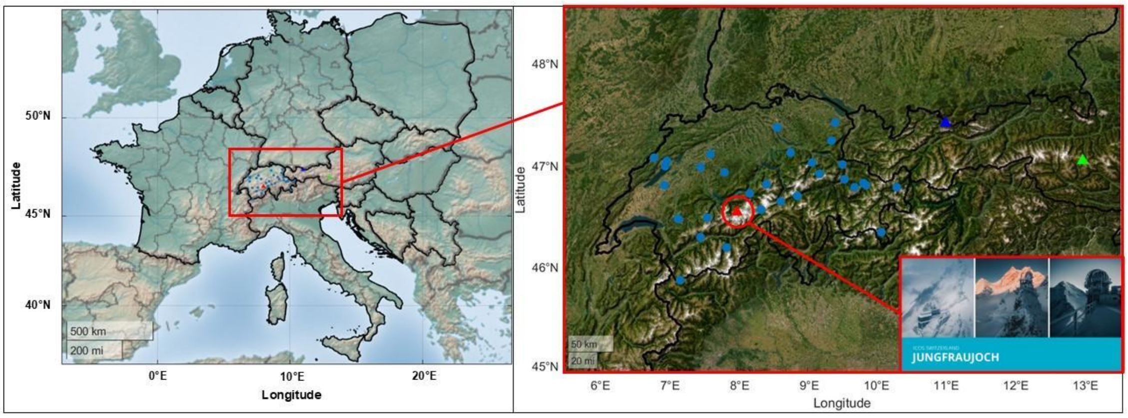

Figure 1. **Panel Left**: Case study Area. **Panel Right**: Jungfraujoch, Sonnblick and Zugspitze historical meteorological observatories (Red, Green and Blue triangles) and the 30 meteorological stations provided by MeteoSwiss (light blue dots).

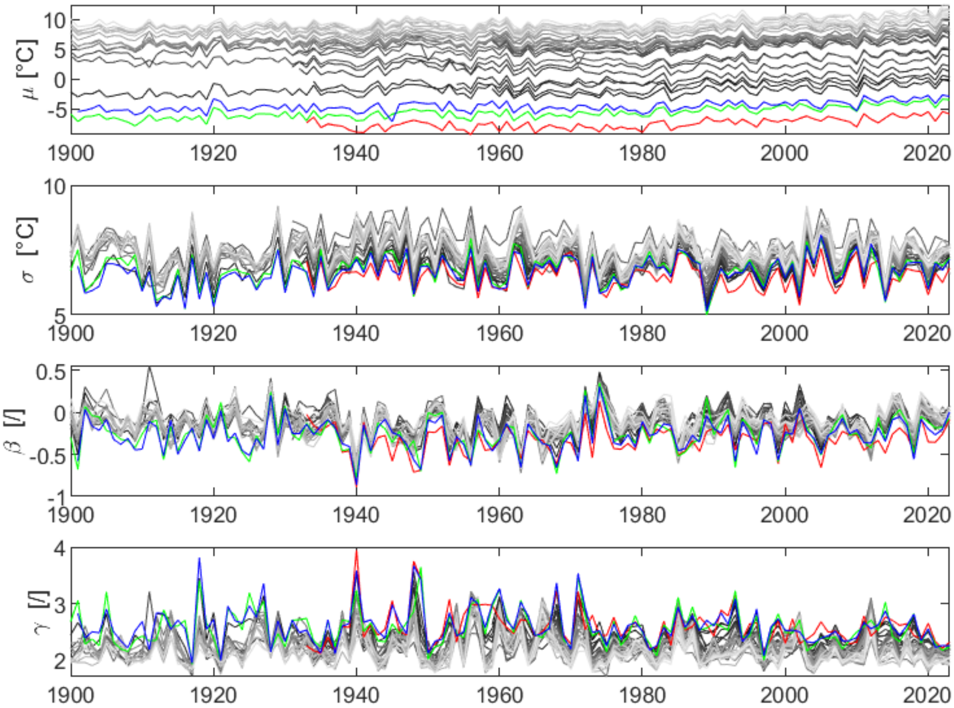

Figure 2. Annual Mean, Standard deviation, Skewness and Kurtosis coefficients (from the top to the bottom) of the observed mean temperature time series about the 30 MeteoSwiss weather stations (grey lines), Zugspitze (blue lines), Sonnblick (green lines), Jungfraujoch (Red lines).

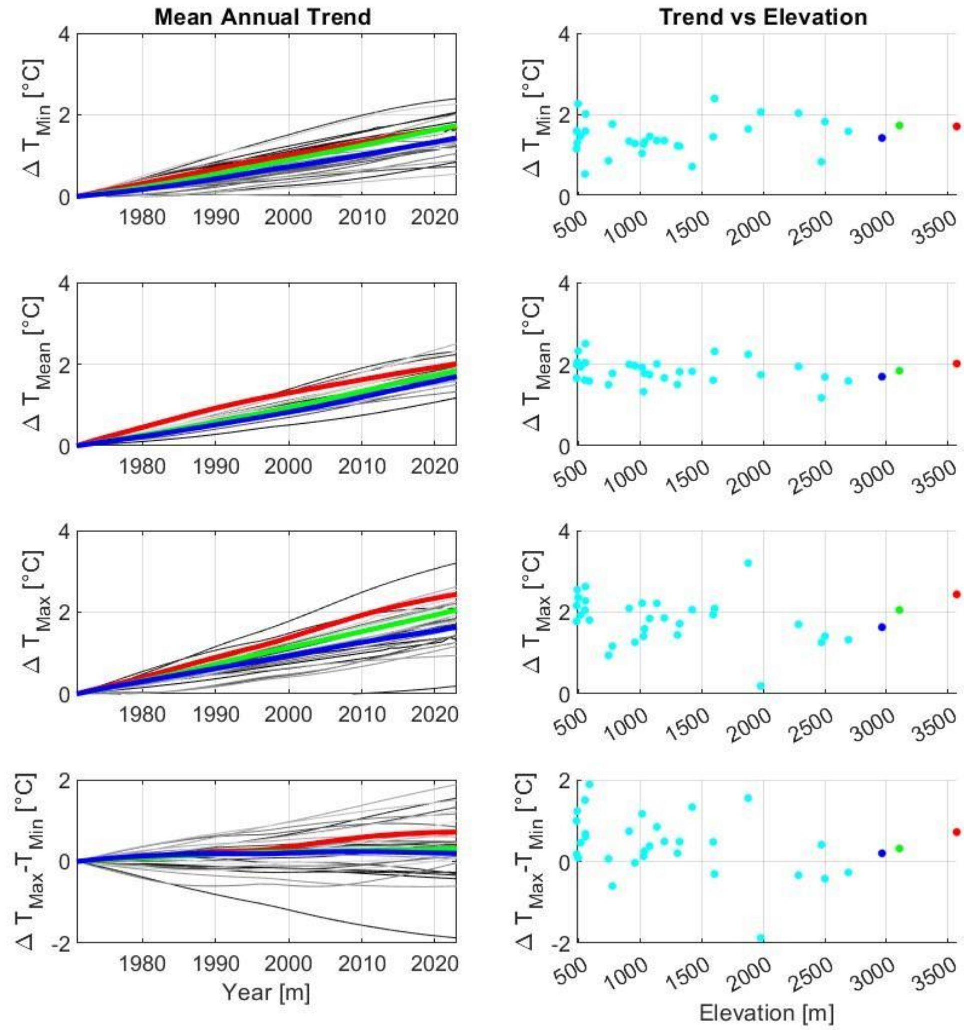

Figure 3. On the left panels: Annual trend of min, mean, max and (max-min) Temperatures time series within the 1971-2023 period about the 33 meteorological stations. On the right panels: The variability of the cumulative trend at the year 2023 versus the stations' elevations.

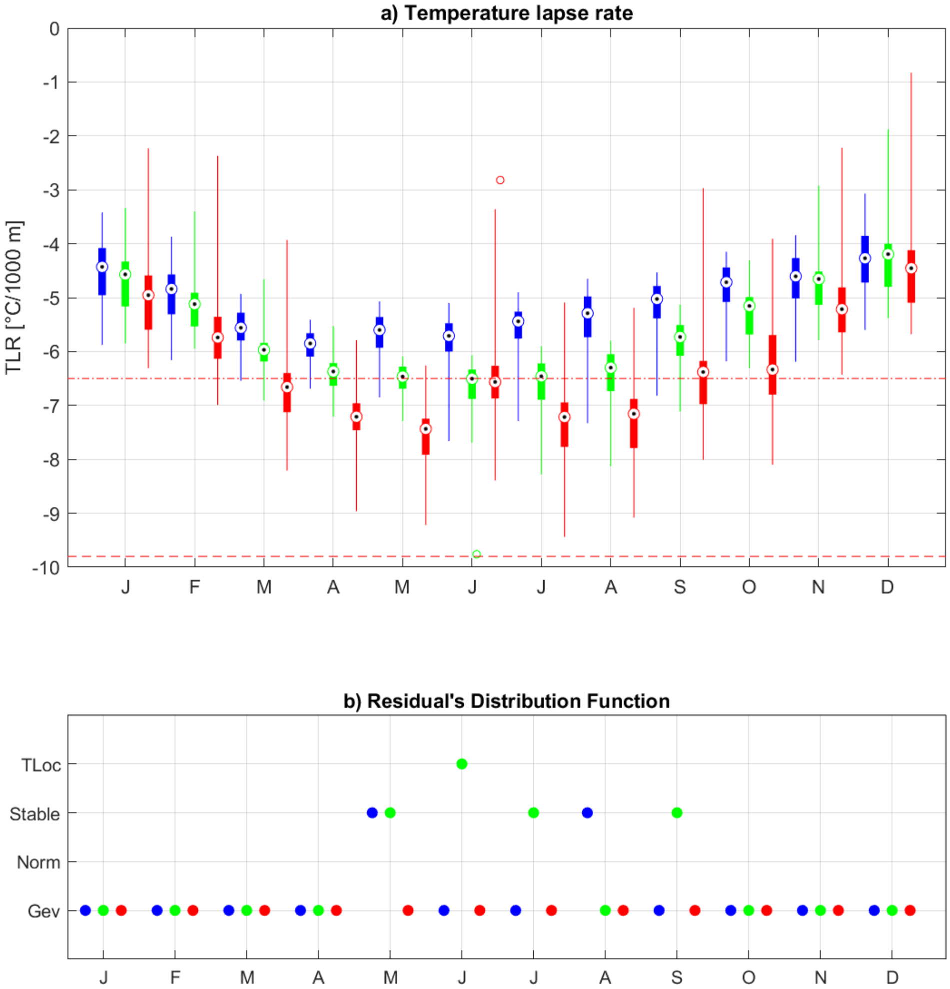

Figure 4. Panel a) TLR boxplot monthly comparison for min (blue), mean (green) and max (red), temperature within the calibration period 1988-2005 for all of the BS meteorological stations (Dashed red lines represent the reference values of the mean Environmental and Dry Adiabatic Lapse Rates). Panel b) Residuals' statistical distribution function (the mode among the 30 pairwise BS-TS) monthly variability in the calibration period.

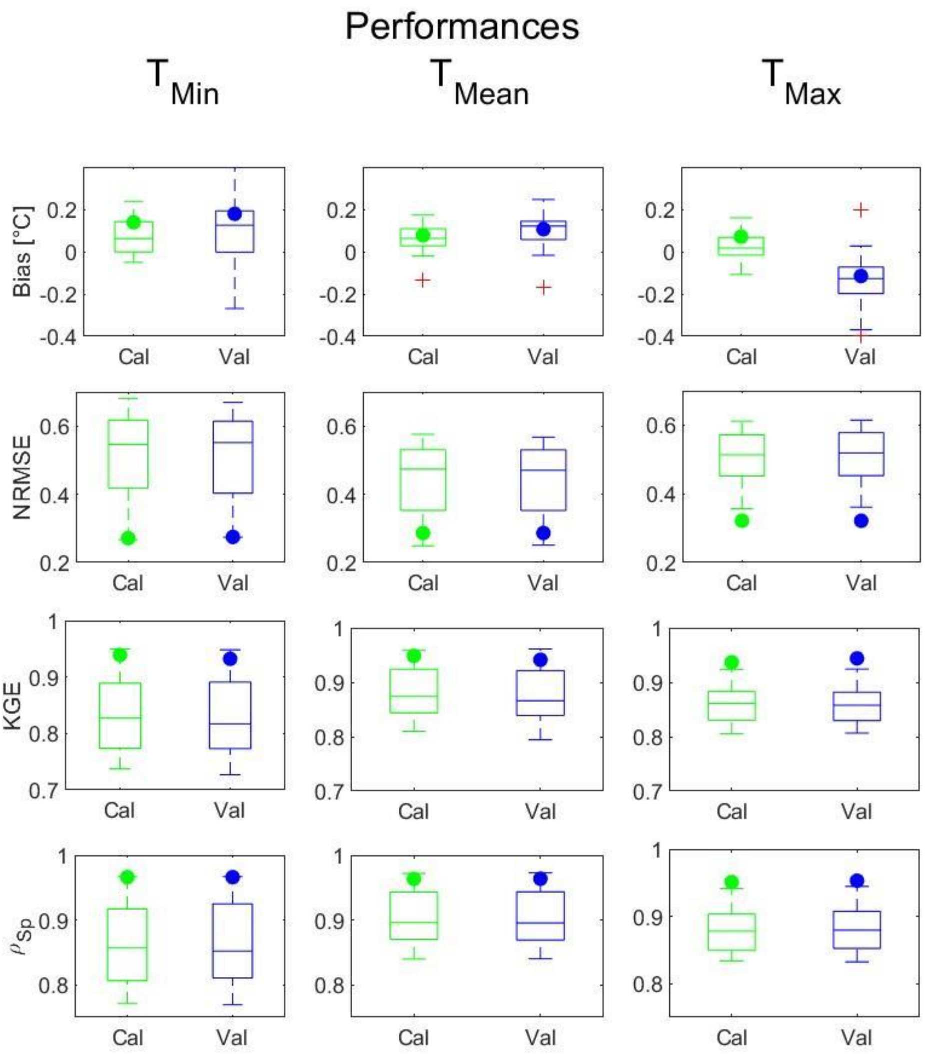

Figure 5. Comparison of the model's performances (Bias, NRMSE, KGE, Spearman correlation coefficient) between calibration (green) and validation (blue) periods. The boxplots represent the 32 BS stations, the dots are the Ensemble simulations. Panels left, central and right refer respectively to Min, Mean and Maximum Temperature.

.

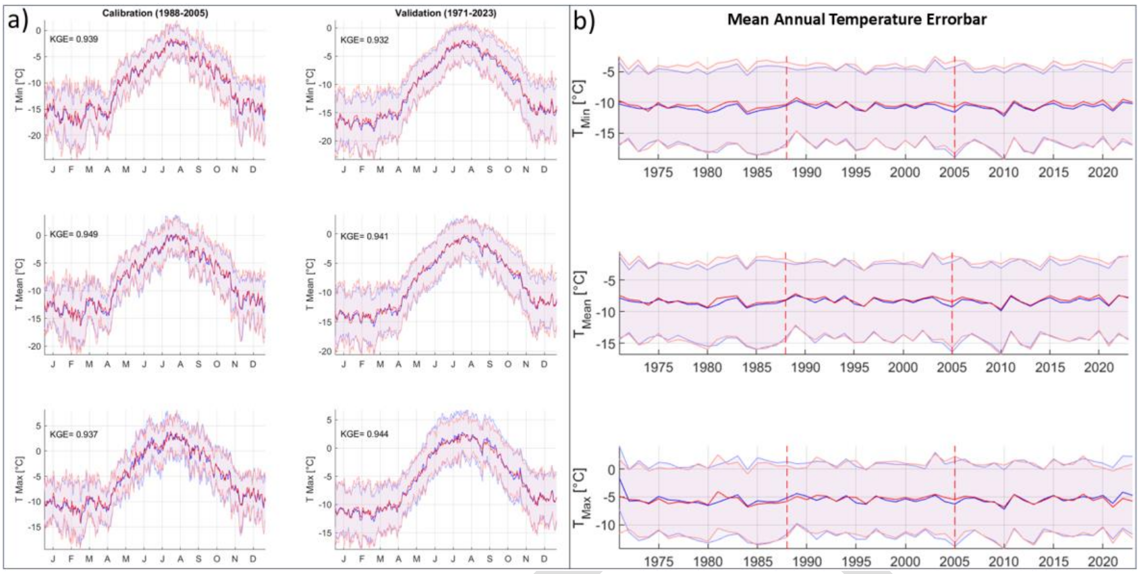

Figure 6. Comparison between the ensemble simulation (blue) and observation (red) in both calibration and validation periods. Panel a: Daily Error bar with KGE coefficients. Panel b: Annual error bar with the subdivision of calibration and validation periods.

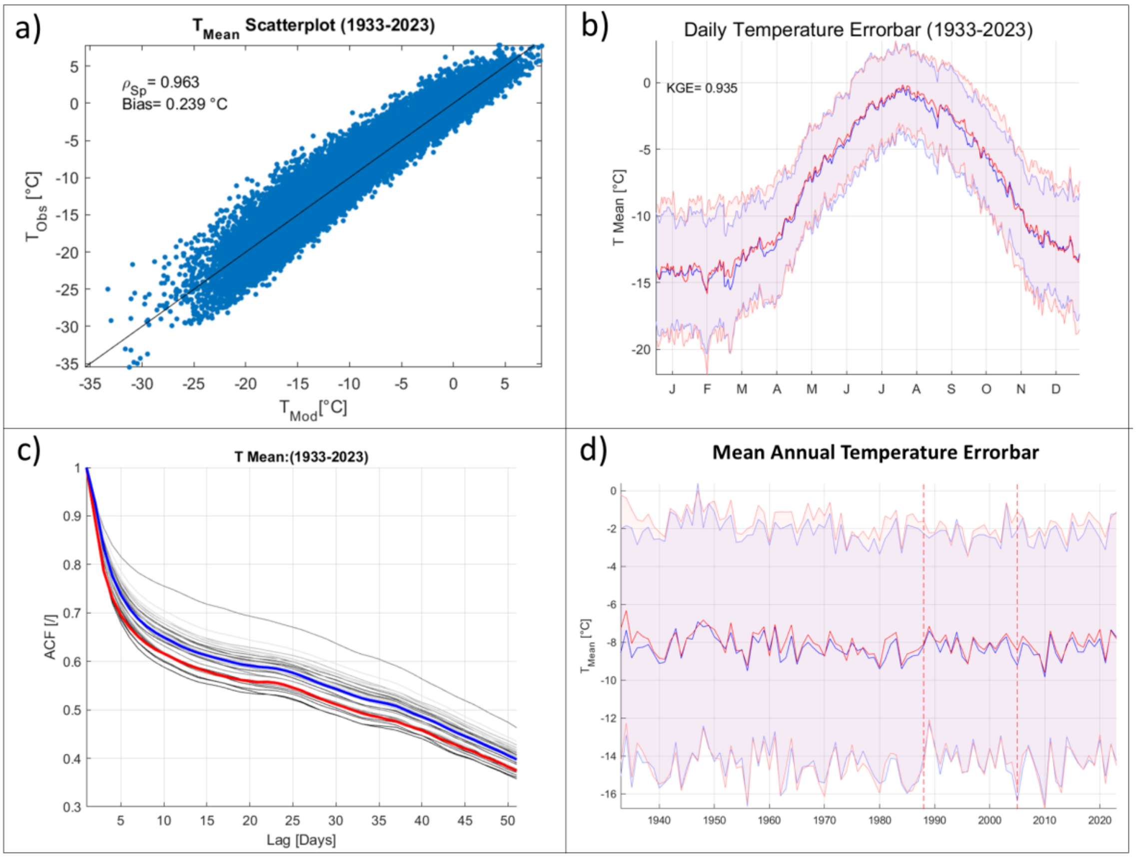

Figure 7. Comparison between Ensemble (blue) and observed (red) Daily Mean Temperature in the period 1933-2023. Panel a) Scatterplot with bias and Spearman correlation coefficients; Panel b) Daily error bar with KGE value; Panel c) Autocorrelation function (50 days of lag); Panel d) 1933-2023 Annual error bar time series.

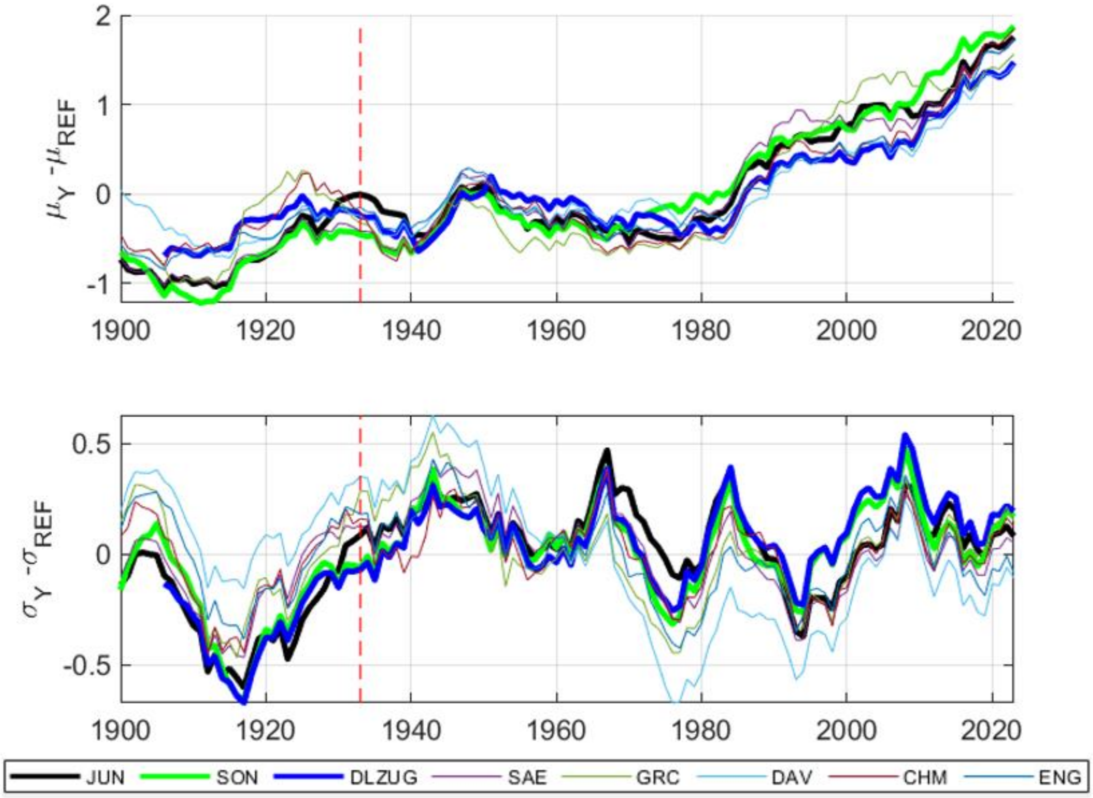

Figure 8. Mean (top panel) and standard deviation (bottom panel) anomalies comparison related to the 8 stations located at Elevation greater than 1000 m a.s.l. The lines represent the 10 years moving average anomalies (where the anomaly is the difference between the yearly value and the mean of the period 1900-2023). Heavy lines represent the 3 historical observatories of Jungfraujoch, Sonnblick and Zugspitze, thin ones the other 5 Swiss sites.With red dashed line we distinguish the 1900-1933 period (Ensemble estimation) and 1933-2023 (observation).